Наносистеми, наноматеріали, нанотехнології
Nanosistemi, Nanomateriali, Nanotehnologii
2025, т. 23, № 4, сс. 1115–1127
https://doi.org/10.15407/nnn.23.04.1115

PACS numbers: 68.37.Hk, 68.37.Vj, 78.20.Ci, 78.40.Fy, 78.67.Sc, 81.16.Pr, 82.30.Lp

Effect of Substrate Temperature on the Optical Properties of Copper-Oxide Nanostructured Thin Films by Chemical Spray Pyrolysis

Omar Ayed and Mushtaq Abed Al-Jubbori

College of Education for Pure Sciences,
Department of Physics,
University of Mosul,
41001 Mosul, Iraq

Nanostructured thin copper-oxide (CuO) films are grown by the chemical spray pyrolysis (CSP) technique. Utilising a homemade spray pyrolysis method, thin films are created. This work investigates the role of the gamma and ultraviolet rays' irradiation in the optical properties of thin CuO films prepared. In this framework used different substrate temperatures of 300, 350 and 400°C, the layers are grown on glass for the prepared thin CuO films. UV-visible spectrometer and field-emission scanning electron microscopy (FE-SEM) are used to characterize the samples. The UV-visible spectroscopy shows a decrease in the absorbance and the optical band gap of thin CuO films with the increase in the higher substrate temperatures. Additionally, surface-plasmon resonance peaks (λ_{SPR}) is observed at 329 nm. FE-SEM images reveal spherical-like shapes with an average diameter range of 48 nm, 56 nm and 62 nm for 300, 350 and 400°C, respectively.

Наноструктуровані тонкі плівки оксиду Купруму (CuO) були вирощені методом хемічної розпорошувальної піролізи. З використанням саморобного методу розпорошувальної піролізи було створено тонкі плівки. У цій роботі досліджувалася роль гамма- й ультрафіолетового випромінювання в оптичних властивостях одержаних тонких плівок CuO. Використовувалися різні температури підкладинки: 300, 350 і 400°C, за яких вирощувалися шари на склі для одержаних тонких плівок CuO. Для характеризації зразків використовувалися спектрометер УФ- й видимого діяпазонів і польова емісійна сканівна електронна мікроскопія (FE-SEM). УФ- й видима спектроскопія показала зменшення вбирання та ширини забороненої зони тонких плівок CuO зі збільшенням температури підкладинки. Крім того, спостерігалися піки поверхневого плазмонного резонансу (λ_{SPR}) за 329 нм. Зображення, одержані методом FE-SEM, виявили сферичні форми із середнім діяпазоном діяметрів у 48 нм, 56 нм і 62 нм для 300, 350 і 400°C відповідно.

Key words: CSP technique, substrate temperature, optical properties, FE-SEM.

Ключові слова: метод хемічної розпорошувальної піролізи, температура підкладинки, оптичні властивості, польова емісійна сканівна електронна мікроскопія.

(Received 20 May, 2024; in revised form, 2 June, 2024)

1. INTRODUCTION

Synthesis of copper-oxide (CuO) nanoparticles has achieved through various techniques, and they can be doped with other nanoparticles to form composites. CuO has a wide range of applications in biomedicine, industry, and environmental remediation, has gained increasing attention in various biomedical and industrial sectors due to its physicochemical properties [1, 2]. Copper oxides, specifically CuO_2 and CuO, hold significance as semiconductor materials due to their intrinsic properties and diverse applications. Cu_2O is used in optical energy utilization fields like photovoltaic, photocatalysis, photodegradation, showcasing its importance in these areas [3, 4].

On the other hand, CuO acts as a corrosion inhibitor and a *p*-type semiconductor, making it valuable for various applications such as batteries, solar cells, sensors, and catalysis [5]. The unique characteristics of copper oxide, including high chemical stability, non-toxicity, and cost-effectiveness, contribute to its appeal as a semiconductor material for optoelectronic devices [6]. Additionally, the redox mechanism of copper-oxide compounds, along with their stable physical and chemical properties make them suitable for the preparation of high-performance supercapacitors, further highlighting their importance in the semiconductor industry [7].

Recently, there has been a significant interest in metallic nanoparticles across various fields. Their distinct properties have led to applications in chemical imaging [8], solar cells [9], organic molecule adsorption, sensors and biosensors [8] and surface-enhanced Raman scattering [10]. Spray pyrolysis (SP) is an efficient, simple, and cost-effective technique to synthesis high-quality thin films compared to other deposition routes [11]. A common method for creating particles is spray pyrolysis, which involves breaking down precursor molecules at a high temperature. It is comparable to combustion in theory, in which liquid fuel oxidizes to produce gases and particles. The only distinction is that while combustion creates polluting particles, spray pyrolysis yields beneficial powders [12]. The components of a standard spray pyrolysis system include a reactor, collection unit, droplet generator, and reservoir for the pre-

cursor solution. A gas atomizes precursor solutions of aqueous or non-aqueous solvents, carrying the droplets into a reactor where they evaporate and solidify into particles [13]. Particle formation also involves the growth and nucleation of the monomer precursor. Heat is provided by an electrical heating source or flame to aid in the solvents' evaporation and precursors' breakdown.

There are different types of chemical spray pyrolysis (CSP) units based on the type of pyrolysis reaction and nozzle used in spraying the solutions. The nature of thin film obtained from SP depends on various parameters and hence, parameters play a vital role in thin film growth. SP plays an important role in the synthesis of metal oxide film formations, which are used in a variety of fields such as supercapacitors. The technique involves spraying a solution onto a substrate, which then undergoes pyrolysis to form a thin film Spray pyrolysis can be used to thin films, such as CuO. SP offers advantages such as ability to deposit thin films of various thicknesses [12, 14]. The principles underlying this method rely on the ability to obtain liquid solutions from primary materials that can thermally react with each other upon spraying to produce the desired membrane. The method offers speed and simplicity in comparison to other preparation techniques, as it does not require advanced technologies or multiple devices. Furthermore, the design of the apparatus used is straightforward and does not necessitate the presence of a vacuum space during the preparation process. Additionally, thin membranes with relatively large areas can be easily prepared, unlike in other techniques [15]. The optical properties characterized by surface plasmon resonance (SPR) hold specific significance. SPR refers to the collective oscillation of electrons within the conduction band in reaction to the electrical field of incident light. The SPR is contingent upon the particles' size, shape, and geometry. These variables influence the sensitivity of nanoparticles [16].

In this paper, copper-oxide nanoparticles have been synthesized using thermal chemical spraying technique at various substrate temperatures. The prepared samples were examined by UV-Visible spectroscopy and FE-SEM to revel their optical and topographical properties of thin films prepared.

2. EXPERIMENTAL DETAILS

2.1. Sample Preparation

The preparation of copper-oxide (CuO) films' solution involves the utilization of cupric chloride dihydrate, which is a light blue powder $CuCl_2 \cdot 2H_2O$, originating from India and supplied by THOMAS BAKER. Its molecular weight is of 170.48 g/mol. To prepare a so-

lution with a concentration of 0.1 M at room temperature, 1.7048 g of cupric chloride dihydrate is dissolved. The mass of cupric chloride dihydrate is determined using an electronic balance of type Mettler AE-160 with a sensitivity of 10^{-6} g. Samples are prepared in 100 mL of distilled water. The two substances are thoroughly mixed using a magnetic stirrer for 30 minutes to ensure the homogeneity of the solution, resulting in a blue-coloured solution. Glass slides that have been ultrasonically cleaned and cut into tiny pieces are utilized as a substrate for the growth of films.

After that, glass substrates are prepared for deposition by placing them on the surface of an electrically heated heater. The heater is operated according to the specified operating conditions outlined below to obtain thin, uniform, and adherent films of copper oxide (CuO) on the glass substrate. The deposition time is set at 10 sec with a deposition rate of 5 min/ml. There is a pause period of 180 sec after each spray. The vertical distance from the nozzle of the spray device to the substrates is 30 cm. The temperature of the

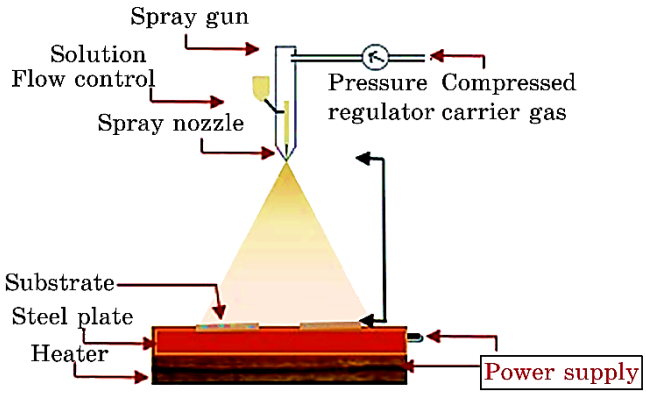

Fig. 1. Experimental setup of the spray pyrolysis technique.

TABLE. Parameters for the spray deposition of the films.

Spray parameters	Optimum value/item
$CuCl_2 \cdot 2H_2O$ solution concentration	0.1 M
Nozzle	Glass
Nozzle-substrate distance	30 cm
Solvent	Distilled water
Carrier gas	Compressed air
Pressure	2 bar
Solution flowrate	5 mL/min
Substrate temperature	300, 350, 400°C

glass substrates is maintained at 300, 350 and 400°C for 10 sprays per temperature, and the air pressure is set at 2 bars. The scheme of the spray pyrolysis in Fig. 1, and film-deposition parameters are listed in Table.

3. RESULTS AND DISCUSSION

3.1. The Optical Absorption Analysis

The interaction of light with thin CuO films can be studied to learn about optical properties. As a result, we used UV-visible spectrophotometry (Shimadzu UV-1800) to characterise the thin CuO films' optical properties with a scanning rate of 400 nm/min; absorbance spectra were obtained from 190 nm to 1100 nm. When light interacts with a thin film, several processes can occur. The optical absorbance *versus* wavelength spectra of the films grown at various substrate temperatures is presented in Fig. 2. All the spectra revealed an optical absorption in the thin films and the absorbance decreases with the increase of substrate temperature. In addition, the spectra showed a steep fall in absorbance at long wavelengths, indicating the presence of a direct optical transition in the films. Further, there was a slight red shift in the absorbance spectra with the increase of substrate temperature. Different temperatures can influence the structural properties, such as crystallinity, grain size, and defect density, which, in turn, affect the optical behaviour of the material.

The surface-plasmon resonance (SPR) peak for the thin CuO films

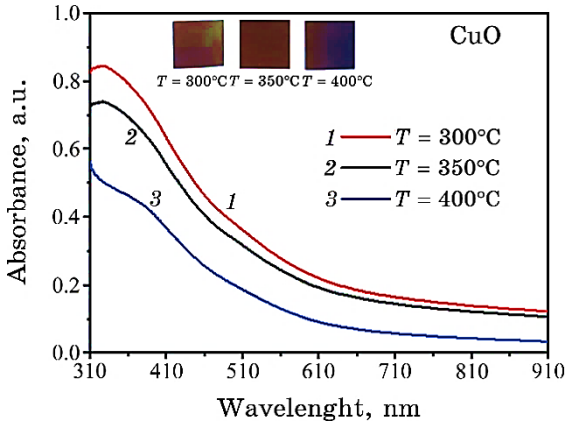

Fig. 2. UV-Vis absorbance curves of CuO films as a function of substrate temperature.

on glass was observed at 329 nm; this peak form is due to the light scattering caused by the CuO film, and the peak position is because there is no agglomeration in the copper-oxide nanoparticles deposited on glass and the interactions between the CuO nanoparticles and the substrates are different. It is worth mentioning that the UV-Vis spectrum for the copper-oxide nanoparticles on glass substrate only shows the SPR peak corresponding to in-plane dipolar.

The higher substrate temperatures during film growth promote better crystallinity and grain growth in the thin film. Improved crystallinity reduces the density of defects such as grain boundaries and dislocations. As a result, the absorption of light by these defect states decreases, leading to lower absorbance overall. In addition, higher substrate temperatures can facilitate smoother film-growth surfaces by promoting better mobility and surface diffusion of nanoparticles. Reduced surface roughness can minimize light scattering and increase light transmission through the film, leading to lower absorbance. In addition, the change in thin CuO films' colour from brown to black is appearing, when increasing the substrate temperature.

The incident photon energy as well as the properties of the material itself have an impact on a material absorption coefficient. According to Beer's law, the transmission (T) and reflection (R) spectra are related to the absorption coefficient [17]:

$$\alpha = \frac{1}{d}\log\left[\frac{(1-R)^2}{2T} + \frac{(1-R)^2}{\left(\sqrt{2T^2+R^2}\right)}\right], \tag{1}$$

where d is the sample thickness. The absorption coefficient (α) at the wavelength of maximum absorption decreases with the increased substrate temperatures of thin CuO films (see Fig. 3).

An important factor affecting a material optical and electronic properties is the optical band gap $E_g^{opt.}$. The optical band gap of the thin copper-oxide films was determined using the Tauc plot and calculated by fitting the equation to the data [18]:

$$(\alpha h\nu)^{1/r} = B\left(h\nu - E_g^{opt.}\right), \tag{2}$$

where r is a number that indicates the type of electronic transition that causes the absorption and takes values of (1/2 or 2/3) for direct transitions and (2 or 3) for indirect ones, depending on whether the transition is allowed or forbidden; $h\nu$ is the photon energy, α is the absorption coefficient, and B is a constant of effective mass (Fig. 4). The optical energy gap decreases with increasing substrate temperatures; this decrease in the optical energy gap is due to the

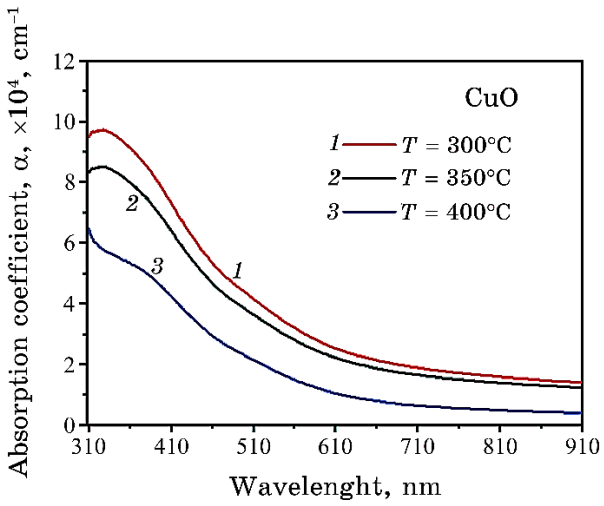

Fig. 3. Absorption coefficient of thin CuO films as a function of wavelength with different substrate temperatures.

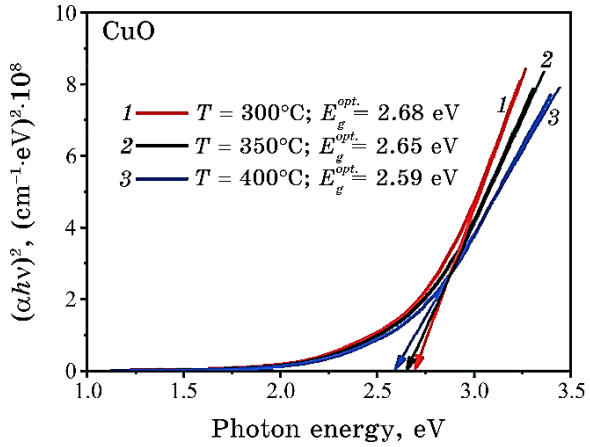

Fig. 4. Optical band gap values for prepared thin CuO films for different substrate temperatures.

increase in the size of CuO nanoparticles for thin films.

The refractive index (n) describes how a beam propagates through a transparent medium. The optical parameters of the samples can be used to determine the refractive index using the relationship [19]

$$n = \left(\frac{1+R}{1-R}\right) + \sqrt{\frac{4R}{(1-R)^2} - K^2}\ . \qquad (3)$$

Reflectivity (R) is calculated from absorption and transmission spectra using the law of conservation of energy: $R = 1 \quad T \quad A$. On the other hand, the extinction coefficient (K) depends on the absorption coefficient and wavelength of the incident beam and is given by Ref. [20]:

$$K = \alpha\lambda/(4\pi)\,. \tag{4}$$

The refractive index and the extinction coefficient against wavelength are given in Eqs. (3) and (4). It can be seen that n and K of thin CuO films decreases with increasing substrate temperatures and in the visible region. When thin films are deposited on a substrate at higher temperatures, they tend to have improved crystallinity and reduced defects. In the case of thin CuO films, increasing the substrate temperature can lead to better crystallization and larger grain sizes that can result in reduced light scattering and absorption. This leads to a decrease in both the refractive index and extinction coefficient, as displayed in Fig. 5.

The complex dielectric constant caused by photon interactions with medium charges is commonly referred to as polarization. Using Maxwell relations, evaluation of the real (ε_r) and imaginary (ε_i) parts of the dielectric constant can be calculated for optical wavelengths based on optical constants. The refractive index and extinction coefficient are connected to the real and imaginary parts of the dielectric constant through the following relationships [21]:

$$\varepsilon_r = n^2 - K^2\,, \tag{5}$$

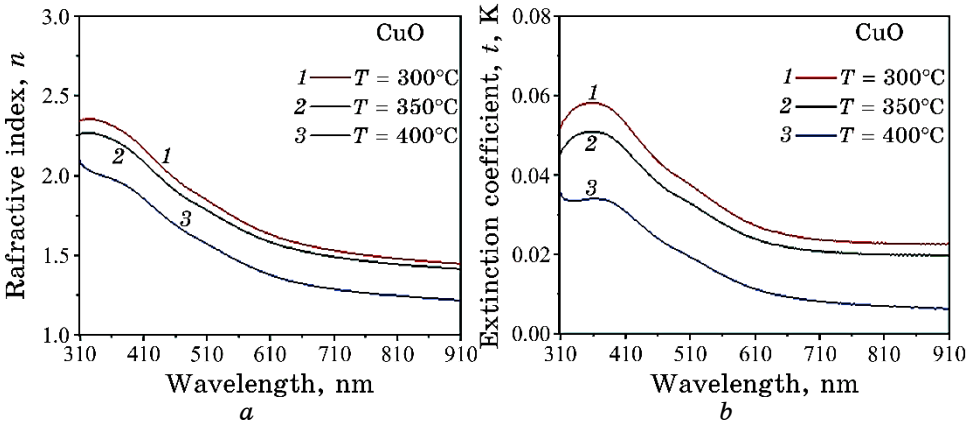

Fig. 5. Refractive index (*a*) and extinction (*b*) coefficient as a function of wavelength for thin CuO films for different substrate temperature.

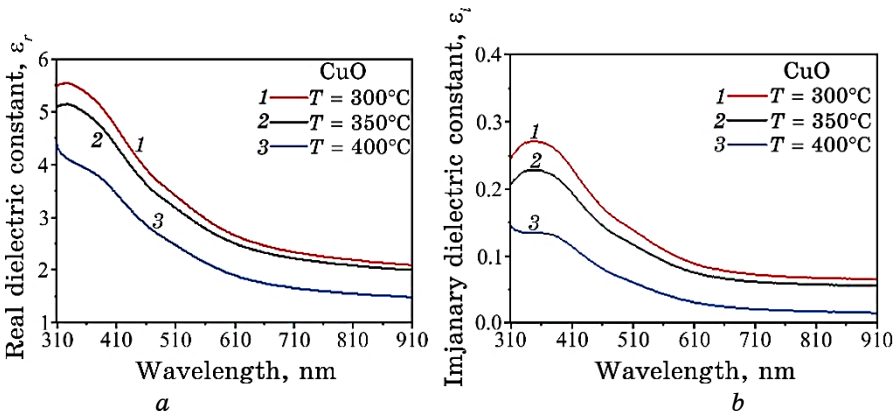

Fig. 6. Real dielectric constants (*a*) and imaginary dielectric constants (*b*) as a function of wavelength for thin CuO films for different substrate temperature.

$$\varepsilon_i = 2nK\,. \tag{6}$$

The real and imaginary dielectric constants of thin copper-oxide films decrease with increasing substrate temperatures and in the visible region as are plotted in Fig. 6. Nanoparticles' size in thin copper-oxide films can be affected by increasing the substrate temperature. The material dielectric properties are impacted by changes in bandgap and carrier concentration, especially, in the visible range. Consequently, the real and imaginary dielectric constants decrease.

The optical conductivity thin CuO films can be determined using the correlation between the absorption coefficient and the refractive index [21]:

$$\sigma_{opt.} = \frac{\alpha nc}{4\pi}\,, \tag{7}$$

where c is the speed of light in a vacuum. The decrease in optical conductivity can be attributed to decrease for absorption coefficient and the refractive index with increasing the substrate temperature, as shown in Fig. 7.

3.2. Field Emission Scanning Electron Microscopy (FE-SEM) Results

Utilizing the FE-SEM analysis at a 200k× magnification, it possible to analyse the morphology and particle size distribution of thin CuO films for different substrate temperature.

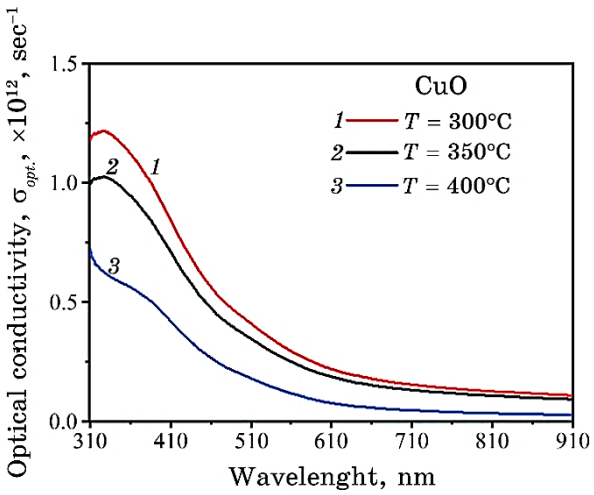

Fig. 7. Optical conductivity as a function of wavelength for thin CuO films for different substrate temperature.

With increasing substrate temperature, the nanoparticles of copper oxide become larger due to the heightened kinetic energy of the particles. This renders them more susceptible to diffusion and coalescence, leading to the formation of larger particles. Consequently, a denser with less porous membrane is formed and exhibiting greater cohesion.

Moreover, the shape of the membrane particles is also affected, as the particles tend to become more spherical with increasing substrate temperature. This is because the increase in temperature that reduces the surface tension on the membrane particles, allowing them to adopt a more stable shape.

The FE-SEM image in Fig. 8 clearly shows those copper-oxide nanoparticles' diameters with a size range of 48 nm, 56 nm and 62 nm for 300, 350, and 400°C, respectively. Finally, the FE-SEM results are in good agreement with the results of UV-Vis analysis.

4. CONCLUSIONS

Thin copper-oxide films can be easily and low-cost produced by chemical spray pyrolysis technique.

The optical properties show that the optical energy gap and the optical constants such as refractive index, extinction coefficient, dielectric constants and optical conductivity decreases with increasing substrate temperature.

In addition, the surface morphology of thin CuO films is a

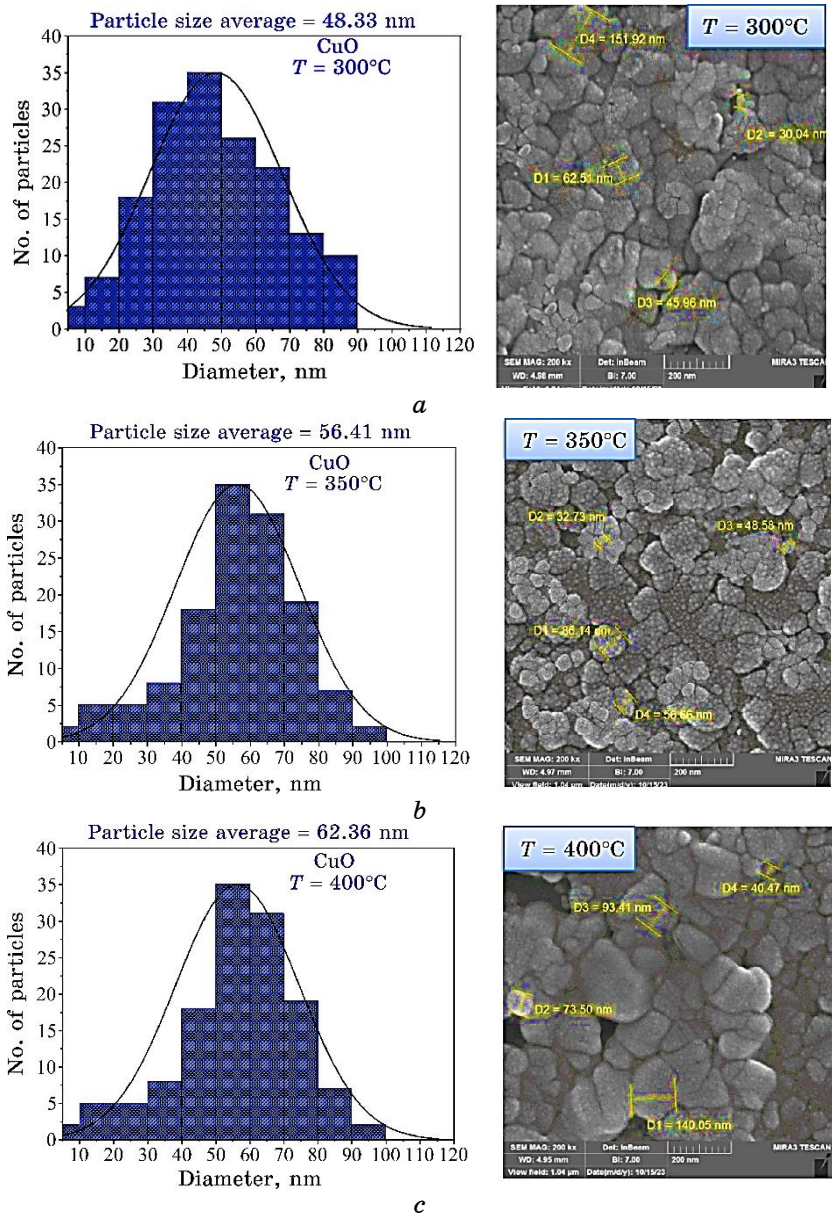

Fig. 8. FE-SEM micrographs of thin CuO films for different substrate temperature and the particle-size distribution for (*a*) 300°C (*b*) 350°C, and (*c*) 400°C.

sphere-like shape and diameters increasing with substrate temperature. The average particles size range of 48 nm, 56 nm and 62 nm for 300, 350 and 400°C, respectively.

ACKNOWLEDGEMENTS

The authors would like to express their warmest thanks to the University of Mosul, College of Education for Pure Science, Department of Physics for supporting this work.

REFERENCES

1. H. Etemadi, J. K. Buchanan, N. G. Kandile, and P. G. Plieger, *ACS Biomaterials Science & Engineering*, **7**, Iss. 12: 5432(2021); https://doi.org/10.1021/acsbiomaterials.1c00938
2. D. Couto, M. Freitas, F. Carvalho, and E, Fernandes, *Current Medicinal Chemistry*, **22**, Iss.15: 1808 (2015); https://doi.org/10.2174/0929867322666150311151403
3. R. B. P. Elmes, K. N. Orange, S. M. Cloonan, D. C. Williams, and T. Gunnlaugsson, *Journal of the American Chemical Society*, **133**, Iss. 40: 15862 (2011); https://doi.org/10.1021/ja2061159
4. R. Bingbing and K. Mindrov, *Bulletin of Science and Practice*, **8**, Iss. 8: 194 (2022); https://doi.org/10.33619/2414-2948/81/25
5. M. Y. El Sayed, N. El Ghouch, G. Younes, and M. S. Awad, *Materials Today Communications*, **35**, Iss. 2: 105490 (2023); https://doi.org/10.1016/j.mtcomm.2023.105490
6. A. M. Patwary, Md. A. Hossain, B. C. Ghos, J. Chakrabarty, S. R. Haque, S. A. Rupa, J. Uddin, and T. Tanaka, *RSC Advances*, **12**, Iss. 51: 32853 (2022); https://doi.org/10.1039/D2RA06303D
7. S. G. Saima, V. A. Shaikh, U. P. Shinde, H. Pavan, and N. Naik, *J. Mater. Sci.: Mater. Electron.*, **34**, Iss. 1361: 14 (2023); https://doi.org/10.1007/s10854-023-10738-7
8. M. A. Gondal, T. F. Qahtan, M. A. Dastageer, T. A. Saleh, Y. W. Maganda, and D. H. Anjum, *Applied Surface Science*, **286**, Iss. 1: 149 (2013); https://doi.org/10.1016/j.apsusc.2013.09.038
9. B. P. Rai, *Solar Cells*, **25**, No. 3: 265 (1988).
10. H. Siddiqui, M. R. Parra, P. Pandey, N. Singh, and F. Z. Haque, *Orient. J. Chem.*, **28**, Iss. 3: 1533 (2012); http://www.orientjchem.org/?p=23212
11. K. Xu, H. Yan, C. F.Tan, Y. Lu, Y. Li, G. W. Ho, and M. Hong, *Advanced Optical Materials*, **6**, Iss. 7: 1701167 (2018); https://doi.org/10.1002/adom.201701167
12. A. P. Yepseu, L. Isac, L. D. Nyamen, F. Cleymand, A. Duta, and P. T. Ndifon, *Journal of Nanomaterials*, **2021**, Iss. 1: 9 (2021); https://doi.org/10.1155/2021/9975600
13. R. S. Kate, H. M. Pathan, R. Kalubarme, B. B. Kale, and R. J. Deokate, *Journal of Energy Storage*, **54**, Iss. 2: 105387 (2022); https://doi.org/10.1016/j.est.2022.105387
14. G. E. Patil, D. D. Kajale, V. B. Gaikwad, and G. H. Jain, *International Scholarly Research Notices*, **2012**, Iss. 2: 5 (2012); https://doi.org/10.5402/2012/275872
15. O. Diachenko, J. Kováč Jr, O. Dobrozhan, P. Novák, J. Kováč, J. Skriniarova, and A. Opanasyuk, *Coatings*, **11**, Iss. 11: 1392 (2021);

doi:10.3390/COATINGS11111392
16. P. Narasu and E. Gutheil, *Fluids*, **7**, Iss. 5: 146 (2022); https://doi.org/10.3390/fluids7050146
17. S. Nie and S. R. Emory, *Science*, **275**, Iss. 5303: 1102 (1997); https://doi.org/10.1126/science.275.5303.1102
18. I. Saini, J. Rozra, N. Chandak, S. Aggarwal, P. K. Sharma, and A. Sharma, *Materials Chemistry and Physics*, **139**, Iss. 2–3: 802 (2013); https://doi.org/10.1016/j.matchemphys.2013.02.035
19. J. Tauc, R. Grigorvici, and A. Vancu, *physica status solidi (b)*, **15**, Iss. 2: 627 (1966); https://doi.org/10.1002/pssb.19660150224
20. M. Rashidian and D. Dorranain, *J. Theor. Appl. Phys.*, **8**, Iss. 2: 121 (2014); doi:10.1007/s40094-014-0121-0
21. A. Kurt, *Turkish Journal of Chemistry*, **34**, Iss. 1: 67 (2010); https://doi.org/10.3906/kim-0903-29
22. K. D. Babu, P. Philominathan, and K. Murali, *Optik*, **186**, Iss. 3: 350 (2019); https://doi.org/10.1016/j.ijleo.2019.03.048